



## Flt3 is a target of coumestrol in protecting against UVB-induced skin photoaging



Gaeun Park<sup>a,b,1</sup>, Sohee Baek<sup>b,c,d,1</sup>, Jong-Eun Kim<sup>a,b,1</sup>, Tae-gyu Lim<sup>a,b,e</sup>, Charles C. Lee<sup>f</sup>, Hee Yang<sup>a,b</sup>, Young-Gyu Kang<sup>g</sup>, Jun Seong Park<sup>g</sup>, Martin Augustin<sup>d</sup>, Michael Mrosek<sup>d</sup>, Chang Yong Lee<sup>f,h</sup>, Zigang Dong<sup>e</sup>, Robert Huber<sup>c,i,j,k</sup>, Ki Won Lee<sup>a,b,1,\*</sup>

<sup>a</sup> WCU Biomodulation Major, Department of Agricultural Biotechnology, Seoul National University, Seoul, Republic of Korea

<sup>b</sup> Advanced Institutes of Convergence Technology, Seoul National University, Suwon, Republic of Korea

<sup>c</sup> Max Planck Institute for Biochemistry, Martinsried, Germany

<sup>d</sup> Proteros Biostructures GmbH, Martinsried, Germany

<sup>e</sup> The Hormel Institute, University of Minnesota, Austin, Minnesota, United States

<sup>f</sup> Department of Food Science, Cornell University, Ithaca, New York, United States

<sup>g</sup> Skin Research Institute, Amorepacific Corporation R&D Center, Yongin, Republic of Korea

<sup>h</sup> Department of Biochemistry, King Abdulaziz University, Jeddah, Saudi Arabia

<sup>i</sup> Department of Chemistry, Technical University of Munich, Garching, Germany

<sup>j</sup> School of Biosciences, Cardiff University, Wales, UK

<sup>k</sup> Center for Medical Biotechnology, University of Duisburg-Essen, Essen, Germany

<sup>1</sup> Institute on Aging, Seoul National University, Seoul, Republic of Korea

### ARTICLE INFO

#### Article history:

Received 27 April 2015

Accepted 19 August 2015

Available online 2 September 2015

#### Keywords:

Coumestrol

Photoaging

Matrix metalloproteinase 1

FLT3 kinase

### ABSTRACT

While skin aging is a naturally occurring process by senescence, exposure to ultraviolet (UV) radiation accelerates wrinkle formation and sagging of skin. UV induces skin aging by degrading collagen via activating matrix metalloproteinases (MMPs). In this study, we show that coumestrol, a metabolite of the soybean isoflavone daidzein, has a preventive effect on skin photoaging in three-dimensional human skin equivalent model. Coumestrol inhibited UVB-induced MMP-1 expression and activity. Whole human kinase profiling assay identified FLT3 kinase as a novel target protein of coumestrol in UVB-induced signaling pathway in skin. Coumestrol suppresses FLT3 kinase activity, and subsequently, Ras/MEK/ERK and Akt/p70 ribosomal S6 kinase pathway. This suppresses AP-1 activity and in turn, diminishes MMP-1 gene transcription. Using X-ray crystallography, the binding of coumestrol to FLT3 was defined and implied ATP-competitive inhibition. Residues Lys644 and Phe830 showed local changes to accommodate coumestrol in the ATP-binding pocket. 4-APIA, a pharmacological inhibitor of FLT3, inhibited MMP-1 expression and induced signal transduction changes similar to coumestrol. Taken together, coumestrol inhibits UVB-induced MMP-1 expression by suppressing FLT3 kinase activity. These findings suggest that coumestrol is a novel dietary compound with potential application in preventing and improving UVB-associated skin aging.

© 2015 Elsevier Inc. All rights reserved.

### 1. Introduction

Skin aging is a naturally occurring process by senescence, but is also affected by environmental stress such as sunlight, air pollution, and extreme temperature which causes premature skin aging [1,2]. In particular, ultraviolet (UV)B radiation from the

sunlight is the major cause of exacerbated skin aging and leads to skin damage such as sunburn, immune-suppression, photoaging [3], and photo-carcinogenesis [4].

Exposure to UVB alters biological processes that promote matrix metalloproteinases (MMPs) expression, decrease procollagen synthesis, and increase connective tissue damage [2,5,6]. These complex changes trigger wrinkle formation throughout the various layers of skin, but the major changes occur in the dermis [7,8]. MMP-1 is a type of collagenase, which breaks down collagen fibrils. Repeated UVB exposure increases the level of MMP-1 in the dermis and dermal fibroblasts, and therefore triggers histopathological changes [5,6,8]. MMP-1 expression is mediated by cellular

\* Corresponding author. Department of Agricultural Biotechnology, Seoul National University, Seoul, Republic of Korea. Fax: +82 2 873 5095.

E-mail address: [kiwon@snu.ac.kr](mailto:kiwon@snu.ac.kr) (K.W. Lee).

<sup>1</sup> These authors contributed equally to this work.

signaling transduction such as mitogen-activated protein kinase (MAPK) and phosphatidylinositol 3-kinase (PI3K)/Akt [9,10] pathways. These signaling cascades elevate activator protein 1 (AP-1) activity and enhance MMP-1 gene transcription.

Coumestrol (Fig. 1A), one of the soybean isoflavonoids, belongs to the coumestan family [11,12]. Under stress such as germination, fungal infection, or chemical elicitors, coumestrol is produced as a phytoalexin through the conversion of daidzein (Fig. 1B), the aglycon of daidzin (Fig. 1C) [13,14]. Although less studied, coumestrol has a higher antioxidant activity than the major soybean isoflavones including daidzein and genistein [15–17]. Recent reports showed that coumestrol exerts anti-cancer, anti-obesity, and neuroprotective effects without significant side effects [18–20]. In this study, we investigated the potential protective effect of coumestrol against UVB-induced skin photoaging and aimed to uncover the direct molecular target of coumestrol.

## 2. Materials and methods

### 2.1. Chemicals and reagents

Coumestrol, daidzin, daidzein, FBS, and  $\beta$ -actin antibody were obtained from Sigma–Aldrich (St. Louis, MO). DMEM was purchased from Hyclone (Long, UT). MMP-1 antibody was obtained from R&D Systems Inc. (Minneapolis, MN). Antibodies against phosphorylated ERK1/2 (Thr<sup>202</sup>/Ty<sup>r204</sup>) and total ERK1/2 were purchased from Santa Cruz Biotechnology (Santa Cruz, CA). The other antibodies were obtained from Cell Signaling Biotechnology

(Danvers, MA). Penicillin/streptomycin was purchased from Life technologies (Carlsbad, CA). 4-(4-Aminophenyl)-1H-indazol-3-ylamine (3-aminoindazole compound) was obtained from MERCK Millipore (Nottingham, UK).

### 2.2. Cell culture and UVB irradiation

Human dermal fibroblasts (HDFs) were isolated from the outgrowth of foreskin obtained from 7 to 30 year old healthy volunteers from Dr. J.H. Chung's laboratory at Seoul National University (SNU) Hospital (Seoul, South Korea) under the Institutional Review Board at SNU Hospital and SNU. HDFs were cultured in DMEM with 10% (v/v) FBS and 1% (v/v) penicillin/streptomycin at 37 °C and 5% CO<sub>2</sub>. Serum-starved monolayer cultures of HDFs were exposed to UVB at a dose of 0.02 J/cm<sup>2</sup> using UVB source (Bio-Link crosslinker, Vilber Lourmat, Cedex 1, France) set spectral peak at 312 nm.

### 2.3. 3D human skin equivalent system

Using Neoderm<sup>®</sup>-ED purchased from TEGO Science (Seoul, South Korea), we generated the 3D human skin equivalent system. Briefly, HDFs were cultured in collagen matrix for 1 day. Keratinocytes were then seeded on top of collagen matrix and co-cultured for 4 days. Next, the keratinocytes and HDF blocks were lifted and allowed to be exposed to air. Coumestrol, daidzin, and daidzein were treated for 1 h after 2 weeks of the air-lift. Prepared 3D human skin blocks were irradiated with 0.05 J/cm<sup>2</sup> UVB twice a day for 8 days. During this period, the medium was changed every 2 days and the blocks were incubated at 37 °C and 5% in a CO<sub>2</sub> atmosphere.

### 2.4. Cell viability

The cell viability was measured using the CellTiter 96<sup>®</sup> AQueous One Solution Cell Proliferation Assay (Promega, Madison, WI) following the manufacturer's instructions.

### 2.5. Histological examination

3D human skin equivalent blocks were fixed with 10% neutral-buffered formalin, and embedded in paraffin. We sectioned the paraffin block (4  $\mu$ m thickness) and transferred them onto slides. After deparaffinization, the sections were stained with hematoxylin and washed and stained in bieberich scarlet and acid fuchsin. Next, the slides were placed in phosphomolybdic-phosphotungstic acid and then in aniline blue to stain collagen, and washed and incubated in 1% acetic acid. After dehydration and washing, the sections were examined at 400 $\times$  magnification using an Olympus AX70 light microscope (Tokyo, Japan).

### 2.6. Immunohistochemical staining

3D human skin equivalent blocks were fixed, embedded, and deparaffinized as described above. The slides were incubated in 0.3% hydrogen peroxide to remove the endogenous peroxidases and blocked using 5% normal goat serum. After blocking, the slides were incubated with MMP-1 antibody at 4 °C overnight. Next, they were reacted to biotinylated secondary antibody (Vector Labs, Burlingame, CA) and developed using avidin–biotin complex kit (Vector Labs). The reaction was visualized with 3,3'-diaminobenzidine tetrahydrochloride hydrate solution (Vector Labs). The counterstain was conducted using hematoxylin. The level of MMP-1 was examined under 400 $\times$  magnification. To evaluate collagen status in the dermis, Masson's trichrome staining was performed. Mouse skin samples and human skin equivalents were fixed with

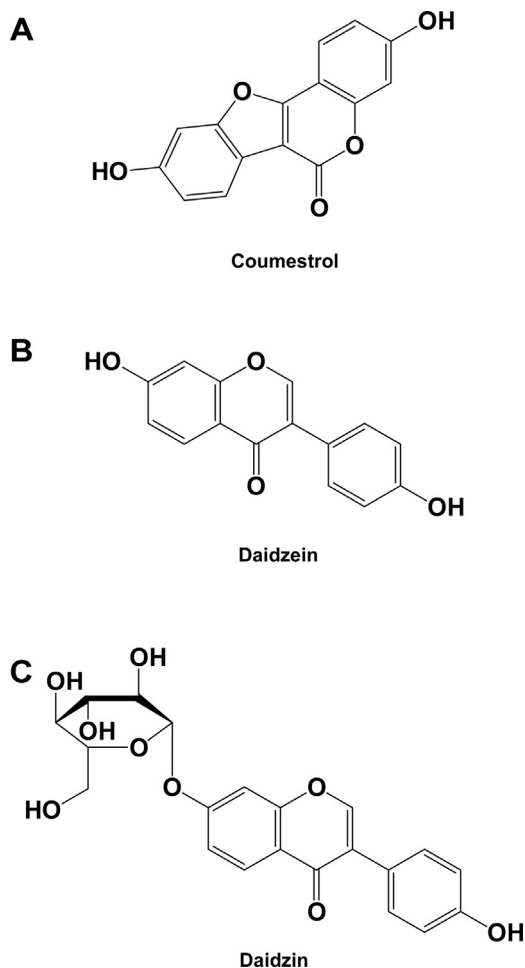


Fig. 1. Chemical structure of coumestrol, daidzin, and daidzein.

10% neutral-buffered formalin, and embedded in paraffin. Serial sections (4  $\mu\text{m}$  intervals) were then mounted onto slides. After deparaffinizing, skin sections were stained with hematoxylin for 5 min, before being washed and stained in bieberich scarlet and acid fuchsin. The slides were then placed in phosphomolybdic-phosphotungstic acid for 10 min and aniline blue for 5 min to stain the collagen. Slides were then washed and incubated in 1% acetic acid for 15 min. Lastly, they were dehydrated and washed. Skin sections were examined at 400 $\times$  magnification using an Olympus AX70 light microscope (Tokyo, Japan).

### 2.7. MMP-1 content and activity measurement

MMP-1 content in the conditioned medium of HDFs was measured by DuoSet human total MMP-1 ELISA kit (R&D system Inc.) and MMP-1 activity was measured by using Sensolyte 520 MMP-1 assay kit (AnaSpec Inc., Fremont, CA) according to the manufacturer's instructions.

### 2.8. Real-time RT-PCR

HDFs were treated with coumestrol for 12 h and harvested in RNAiso Plus (Takara Bio Inc., Shiga, Japan). After reverse transcription with oligo-dT primers using a PrimeScript<sup>TM</sup> 1st strand cDNA synthesis Kit (Takara Bio Inc.), real-time RT-PCR was performed using IQ SYBR (Bio-Rad Laboratories). Side-strand-specific primers for MMP-1, GAPDH were as follows: MMP-1 forward (5'-CCC CAA AAG CGT GTG ACA GTA-3'); MMP-1 reverse (5'-GGT AGA AGG GAT TTG TGC G-3'); GAPDH forward (5'-GAG TCA ACG GAT TTG GTC GT-3'); GAPDH reverse (5'-TTG ATT TTG GAG GGA TCT CG-3').

### 2.9. AP-1 reporter gene assay

HDFs were co-transfected with 0.5  $\mu\text{g}$  of Renilla vector, 5  $\mu\text{g}$  of luciferase gene expression vectors containing AP-1 binding sequences (TGAC/GTCA) by JetPEI (Polyplus, France). After 9 h of transfection, medium was changed with DMEM-10% FBS for 15 h, and then starved in serum-free DMEM for 24 h. After starvation, the cells were treated with or without coumestrol for 1 h, followed by 0.02 J/cm<sup>2</sup> UVB irradiation. Cell extracts were prepared with reporter lysis buffer (Promega), and the extracts were used for luciferase assay. AP-1 activity in HDFs was determined by using an AP-1 luciferase assay kit (Promega) as described by the manufacturers.

### 2.10. Western blot analysis

HDFs were starved in serum-free DMEM for 24 h and treated with or without coumestrol, daidzin, or daidzein for 1 h, followed by UVB (0.02 J/cm<sup>2</sup>) irradiation. The cells were lysed using RIPA Lysisbuffer (Cell signaling) and the protein concentration was measured using a dye-binding protein assay kit (Bio-Rad Laboratories, Hercules, CA) as described by the manufacturer. The proteins were separated on a 10% SDS-polyacrylamide gel and transferred onto an Immobilon P membrane (MERC Millipore). After blocking, the membrane was incubated with the specific primary antibody at 4 °C overnight. Protein bands were visualized using a chemiluminescence detection kit (GE healthcare, London, UK) after hybridization with the HRP-conjugated secondary antibody (Life technologies).

### 2.11. Zymography

Zymography was performed in 12% polyacrylamide gels in the presence of gelatin (0.1% w/v) as a substrate for MMP-2. The

supernatants were mixed with loading buffer [10% SDS, 25% glycerol, 0.25 M Tris (pH 6.8) and 0.1% bromophenol blue], and run on 12% SDS-PAGE gels without denaturation. The gelatin gels were washed with renaturing buffer (Life technologies) for 1 h at room temperature and incubated for 24 h at 37 °C in developing buffer (Life technologies). After enzyme reaction, the gels were stained with 0.5% Coomassie brilliant blue in 10% Acetic acid and then washed in destaining buffer.

### 2.12. Kinase profiling analysis and FLT3 kinase assay

Kinase profiling analysis was conducted by KinaseProfiler<sup>TM</sup> service (MERCCK Millipore). FLT3 kinase assay was performed following the manufacturer's protocol. Briefly, FLT3 is incubated with 50 mM Tris/HCl (pH 7.5), 150 mM NaCl, 0.1 mM EGTA, 0.03% Triton X-100, 270 mM sucrose, 1 mM benzamidine, 0.2 mM PMSF, 0.1% 2-mercaptoethanol, 100  $\mu\text{M}$  Abtide (EAIYAAPFAK), 10 mM MgAcetate and [ $\gamma$ -33P-ATP]. The reaction was initiated by the addition of the MgATP mix. After incubation for 10 min at 30 °C, the reaction was stopped by the addition of 3% phosphoric acid solution. 10  $\mu\text{l}$  of the reaction was then spotted onto a P30 filtermat and washed three times for 5 min in 75 mM phosphoric acid and once in methanol for 2 min prior to drying and scintillation counting.

### 2.13. Protein expression and purification

FLT3 (amino acids Hs564-958 containing an internal deletion of residues H711-H761) was fused to a DNA sequence coding for an N-terminal thrombin-cleavable HIS-tag and cloned into pFastBac1 (Invitrogen). Recombinant Baculovirus was produced and protein was expressed in Sf9 cells. Cells were harvested and disrupted in 25 mM Tris (pH 8.1), 300 mM NaCl, 15% glycerol, 10 mM imidazole, 5 mM  $\beta$ -mercaptoethanol (buffer A) containing 0.1% TX100, 0.1% octyl glucopyranosid and Complete protease inhibitor cocktails (Roche). The lysate was centrifuged and incubated with Ni-NTA agarose (Qiagen) for 2 h at 4 °C. After washing with buffer A, the protein was eluted with buffer A containing 300 mM imidazole. Cleavage of the His-tag was performed overnight with thrombin at 4 °C and the cleaved protein was recovered by negative-affinity chromatography in buffer A. FLT3 was dialysed in 25 mM Tris (pH 8.1), 25 mM NaCl, 5% glycerol and 5 mM DTT (buffer B) and subsequently, the protein was applied to an ion exchange column (Resource Q; GE Healthcare) in buffer B and eluted with a linear gradient of 0–500 mM NaCl. The eluted protein was further purified using size exclusion chromatography (Superdex 75 26/60; GE Healthcare) in 25 mM Tris (pH 8.1), 500 mM NaCl, 5% glycerol and 5 mM DTT. The peak fractions were concentrated to 9.8 mg/ml using a 10 kDa MWCO concentrator (Amicon Ultra Centrifugal Filter Unit; Millipore).

### 2.14. Crystallization and data collection

Crystallization was performed at 20 °C by the hanging drop vapor diffusion method by mixing protein and reservoir solution at a ratio of 1:1, with the reservoir solution containing 0.20 M LiSO<sub>4</sub>, 0.1 M CAPS (pH 10.0), 0.80 M K<sub>2</sub>HPO<sub>4</sub>, 0.80 M NaH<sub>2</sub>PO<sub>4</sub>. Due to the failure of co-crystallization with coumestrol, apo-crystals were soaked in the well solution supplemented with 5 mM coumestrol for 1 day. A crystal was shock-frozen, with 25% glycerol as cryoprotectant and a data set was collected at 100 K on beamline PXI/X06SA at the Swiss Light Source (SLS, Villigen, Switzerland) and processed using XDS and XSCALE [21] to a resolution of 2.8 Å. The crystal belongs to space group P4<sub>3</sub>2<sub>1</sub>2 with unit cell parameters  $a = b = 81.55$  Å,  $c = 146.31$  Å and contains one FLT3-molecule per asymmetric unit. The final model comprises residues

Gln569–Leu947. The segments not defined by electron density include a loop region (Arg712–Leu780) in accordance with the previously solved apo structure (PDB code 1RJB, [22]).

### 2.15. Structure determination and refinement

The structure of FLT3 in complex with coumestrol was solved by molecular replacement utilizing the published FLT3 apo structure (PDB code 1RJB, [22]) as a search model with the program MOLREP [23] and subsequently improved by iterative cycles of model building in COOT [24] and refinement in REFMAC5, CCP4 [25]. The ligand parameterisation and generation of the corresponding library files were carried out with CORINA. The final R-factor was 20.5% and R-free was 24.4%. The statistics for data collection and refinement are summarized in Table 1.

### 2.16. Reporter displacement assay

The reporter displacement assay was performed as previously described [26]. Briefly, the assay is based on a reporter probe designed to selectively target the FLT3 ATP-binding site. As binding of the reporter probe to the FLT3 generates emission of an optical signal, the displacement of the reporter probe by the compound in question can be quantified through the loss of the optical signal at increasing compound concentrations. The assay was performed in a 384-well black plate. 20 nM FLT3 was mixed with 107 nM ATP site-specific reporter probe in 20 mM MOPS pH 7.0, 1 mM DTT, 0.01% Tween20. After 60 min incubation with the compound, the displacement of the reporter probe was measured with TRF 340/620 nm and 340/665 nm on a PHERAstar.

### 2.17. Statistical analysis

Data was expressed as the means  $\pm$  standard deviation (S.D.). One-way ANOVA with Tukey's HSD test was used to evaluate mean differences of group and statistical significance. Differences were considered significant at  $p < 0.05$ .

**Table 1**  
Data collection and refinement statistics.

Data collection	
X-ray source	PXI/X06SA (SLS) <sup>a</sup>
Space group	P43212
Unit cell parameters	
<i>a</i> , <i>b</i> , <i>c</i> (Å)	<i>a</i> = <i>b</i> = 81.55, <i>c</i> = 146.31
$\alpha$ , $\beta$ , $\gamma$ (°)	90, 90, 90
Resolution (Å)	71.23–2.83
Observed reflections	55,059
Unique reflections	12,197
Completeness (%) <sup>b</sup>	98.0 (97.9)
<i>R</i> <sub>merge</sub> <sup>b</sup>	5.3 (42.7)
<i>I</i> / $\sigma$ ( <i>I</i> ) <sup>b</sup>	21.17 (3.62)
Refinement	
No. of reflections (working/test)	11,526/653
R-factor (%)	20.3
Free R factor (%)	23.7
RMS deviations	0.007
Bond lengths (Å)	
Bond angle (°)	1.13
Bonded B's (Å)	
Total no. of atoms	
Protein	2486
Ligand	20
Water	28

<sup>a</sup> Swiss light source (SLS, Villigen, Switzerland).

<sup>b</sup> Values in parentheses correspond to the highest resolution bin.

## 3. Results

### 3.1. Coumestrol inhibits UVB-induced collagen degradation and collagenase expression in 3D human skin equivalent

To investigate the anti-wrinkle effect of coumestrol, we examined the effect of coumestrol on collagen fibrils and collagenase MMP-1 in 3D human skin equivalent as described in Fig. 2A. After 8 days of UVB irradiation in the presence or absence of coumestrol, paraffin-embedded 3D human skin equivalent were sectioned and subjected to Masson's trichrome stain and immunohistochemistry. Coumestrol inhibited UVB-induced collagen degradation and MMP-1 expression at 20  $\mu$ M, while daidzin and daidzein had little effect (Fig. 2B and C). These results suggest that coumestrol prevents photoaging more effectively than its precursors daidzin and daidzein.

### 3.2. Coumestrol suppresses UVB-induced MMP-1 activity by modulating MMP-1 expression

To investigate how coumestrol prevent collagen degradation, we measured enzyme activity and protein expression levels of MMP-1 using primary human dermal fibroblasts (HDFs). Coumestrol significantly decreased MMP-1 activity compared to the UVB-irradiated and its precursor-treated groups (Fig. 3A). In contrast to daidzin and daidzein, coumestrol markedly reduced UVB-induced MMP-1 protein expression in a dose-dependent manner at 5–20  $\mu$ M (Fig. 3B and C) without affecting cell viability (Fig. 3D). These results suggest that coumestrol modulates MMP-1 activity by suppressing MMP-1 expression.

### 3.3. Coumestrol reduces the FLT3 kinase activity

To find a direct target protein of coumestrol in suppressing UVB-induced signaling pathway, a kinase profiling analysis was conducted by KinaseProfiler™ service (MERCK Millipore). First, 259 kinases activities were analyzed in the presence of 40  $\mu$ M coumestrol (Table 2). Based on this data, we selected 65 kinases whose activities were inhibited more than 80% and further analyzed the selected kinases with 5  $\mu$ M of coumestrol (Table 3). From the kinases which are expressed in human skin according to the protein atlas database [27], we found FLT3 as the main target of coumestrol. To confirm these results, we performed *in vitro* kinase assay which showed that coumestrol strongly inhibited FLT3 kinase activity (Fig. 4A).

### 3.4. Crystal structure and binding kinetics of the FLT3-coumestrol complex

To investigate the molecular basis of the inhibition of FLT3 by coumestrol, we determined the crystal structure of the FLT3-coumestrol complex (Table 1). The FLT3 protein used for structure determination includes the juxtamembrane domain (JM-D), a FLT3 distinct feature [22] responsible for the auto-inhibited conformation observed in the structure. The kinase domain adopts the typical bilobal protein kinase-fold (N- and C- terminal lobes) [28,29] with an ordered activation loop in the DFG-out conformation as it has been described for this crystal form [22]. Superposition of the C $\alpha$ -atoms of our structure and the FLT3 apo-form (1RJB; core rmsd 0.56 Å) using COOT reveals an identical overall structure. However, the FLT3-coumestrol complex shows distinct local changes (Fig. 4D) [22]. Coumestrol binds in the ATP binding pocket between the N- and C- lobes of the kinase and is well defined by electron density (Fig. 4B). Its chromenone-moiety contacts the hinge via H-bonding to the backbone nitrogen of Cys694, and the benzofurano-moiety extends toward the

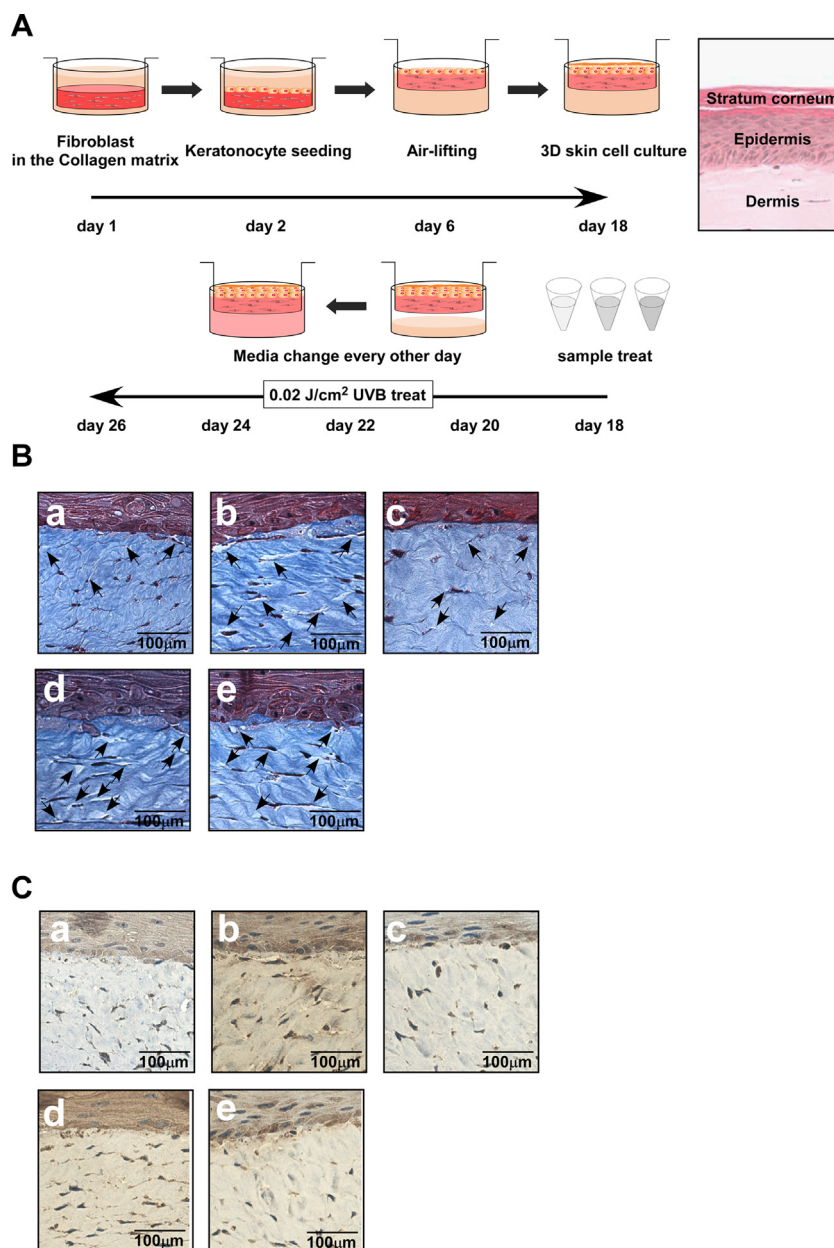


**Fig. 2.** Effect of coumestrol on UVB-induced collagen degradation and MMP-1 expression in 3D human skin equivalent. (A) A schematic diagram of 3D human skin culture system. The experimental procedure is described in Section 2. (B) Representative histological analysis of section of 3D human skin block treated with coumestrol, daidzin, and daidzein (20 μM). Masson's trichrome staining was used to identify collagen fibrils. The arrows indicate degraded collagen (400×, scale bar 100 μm). (C) The level of MMP-1 in 3D human skin block was measured using immunohistochemical staining (400×, scale bar 100 μm). B-C, untreated control (a); UVB (0.05 J/cm<sup>2</sup>) only (b); UVB and coumestrol (c); UVB and daidzin (d); UVB and daidzein (e).

conserved Lys644–Glu661 salt bridge and forms a weak H-bond with Lys644 at a distance of 3.2 Å. These cause a shift of 1 Å of the Lys644 amino group, and the conserved Lys644–Glu661 salt bridge is weakened (2.6 Å in apo-form and 3.4 Å in coumestrol complex). Additional hydrophobic interactions of coumestrol with nonpolar faces of the binding cleft involve Leu616, Val624, Ala642, Val675, Phe691, Tyr693, Gly697, Leu818 and Phe830 (Fig 4C and D). In the coumestrol-bound FLT3-structure, the side chain of Phe830 is slightly displaced from its position in the apo-structure as it would otherwise clash with the bound coumestrol, it is perpendicularly rotated and stabilized by van der Waals interaction, resulting in a small shift of the activation segment main-chain. Overall, the binding of coumestrol to FLT3 is mediated by two hydrogen bonds and hydrophobic interactions in the ATP binding pocket, thus acting in an ATP competitive manner. To measure the binding

kinetics between FLT3 and coumestrol, we performed the reporter displacement assay. The results showed that the IC<sub>50</sub> values of coumestrol and FLT3 inhibitor 4-APIA [30] are 7.55 μM and 3.76 μM, respectively (Fig. 4E and F).

### 3.5. Coumestrol decreases MMP-1 transcription by inhibiting Raf/MEK/ERK and Akt/p70 ribosomal S6 kinase (p70<sup>S6K</sup>) signaling pathways

As we determined FLT3 as a target of coumestrol, we examined the change of down-stream signaling pathway of FLT3 in the presence of coumestrol. UVB-induced FLT3 phosphorylation was not changed by coumestrol treatment (Fig. 5A). FLT3 kinase is an upstream regulator of Raf/MEK/ERK and Akt/p70<sup>S6K</sup> signaling pathways [31–33]. MAPKs and Akt/p70<sup>S6K</sup> have been shown to

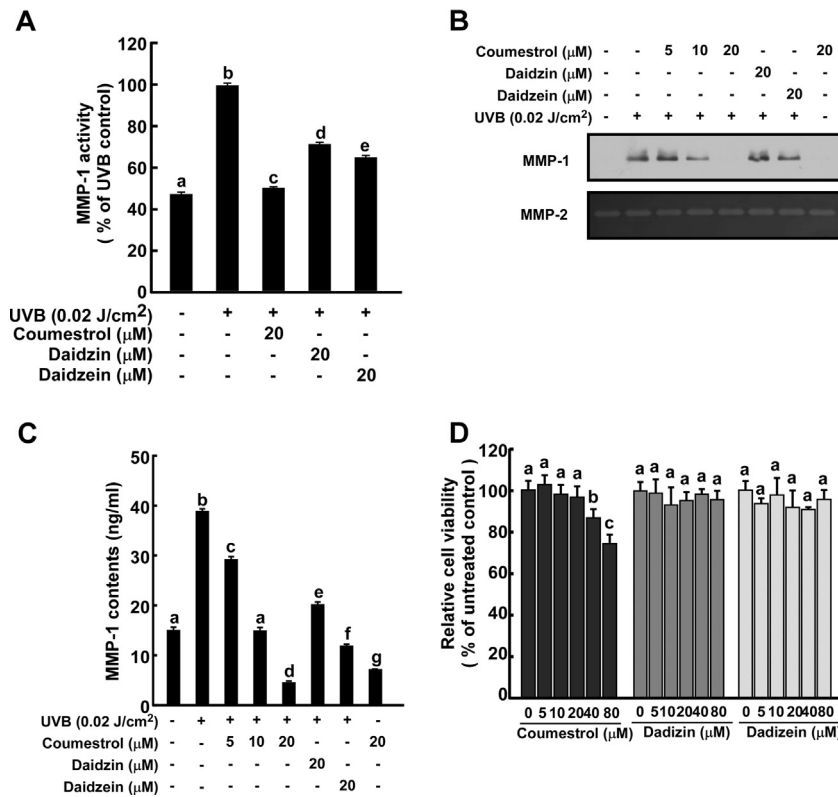


**Fig. 3.** Effect of coumestrol on UVB-induced MMP-1 activity. (A) The level of MMP-1 activity was measured using SensoLyte 520 MMP-1 assay kit at 48 h after UVB exposure. (B) Expression of MMP-1 was determined by Western blot. MMP-2 was used as loading control. Data were representative of triplicate that yielded similar result. (C) The level of MMP-1 was quantified using an ELISA as described in Section 2. (D) The effect of coumestrol, daidzin, and daidzein on cell viability. (A), (C), and (D), data are the means  $\pm$  SD ( $n=3$ ). Means with different letters (a–g) within a graph were significantly different from each other at  $p < 0.05$ .

regulate MMP-1 expression [9,10,34]. Thus, we examined the effect of coumestrol on UVB-induced phosphorylation and total levels of these kinases in HDFs. Coumestrol inhibited UVB-induced phosphorylation of MEK/ERK and Akt/p70<sup>S6K</sup> in a dose-dependent manner (Fig. 5B–D). The alteration of these signal transduction cascades led to the modulation of nuclear transcription factor AP-1 transactivation (Fig. 5E) and finally decreased MMP-1 mRNA transcription (Fig. 5F).

### 3.6. Inhibition of FLT3 kinase diminishes UVB-induced MMP-1 expression through ERK and Akt pathway

To verify the involvement of FLT3 kinase in the UVB-induced MMP-1 expression, we blocked the activation of FLT3 signaling pathway using 4-APIA [30] and identified changes of MMP-1 expression and signaling cascade in HDFs. 4-APIA inhibited UVB-induced MMP-1 expression (Fig. 6A). Moreover, 4-APIA reduced UVB-induced phosphorylation of ERK and Akt (Fig. 6B and C), but not JNK and p38. These results further confirm that the major role of FLT3 kinase in UVB-induced MMP-1 expression and indicate that FLT3 kinase inhibition by coumestrol represents a key regulatory mechanism of coumestrol for inhibiting UVB-induced MMP-1 expression.

## 4. Discussion

UVB plays a key role in triggering skin photoaging. Various MMPs including MMP-1 (collagenase), MMP-3 (stromelysin-1), and MMP-9 (gelatinase B) are increased in human skin or dermal fibroblasts when they are exposed to UVB [5,10,35]. MMP-1 initiates cleavage of fibrillar collagen [36], and once cleaved, collagen fiber can be further degraded by MMP-3 and MMP-9 [37].

Therefore, MMP-1 is regarded as a main enzyme of ECM degradation and wrinkle formation [38], and inhibiting UVB-induced MMP-1 overexpression may have a protective effect against photoaging.

UV irradiation cause reactive oxygen species (ROS) generation and activates membrane receptors of fibroblasts and keratinocytes and signaling pathways to promote MMP-1 expression [39,40]. Previous studies showed that phytochemicals act through ROS scavenging [41]. However, these hypotheses could not explain their specific inhibition effects of signal transduction and their low effective dose. Instead, direct modulatory effects of phytochemicals on their molecular targets could explain their strong bioactivity at low concentration [42]. Our study focuses on identifying the molecular target of coumestrol and confirms its inhibitory effect on downstream effectors.

FLT3 belongs to the class III RTK family including stem cell factor (SCF) receptor (c-Kit), macrophage colony-stimulating factor receptor and platelet derived growth factor receptor A and B [43]. During UVB irradiation, FLT3 ligands, such as SCF, c-kit and others are elevated [44], which bind to the extracellular portion of FLT3. FLT3 forms homodimers and initiates phosphorylation of the Ras/MEK/ERK and PI3K/Akt pathways, in addition to auto-phosphorylating and starting the FLT3 pathway [31–33].

From the kinase profiling data, we suggest FLT3 as a direct target of coumestrol in human skin photoaging protection. The crystal structure of FLT3-coumestrol complex shows that coumestrol binds to the ATP binding site and does not significantly alter the overall structure of the protein. Coumestrol binds to FLT3 by hydrophobic interaction and two hydrogen bonds with residues of ATP-binding site. In addition, the Lys644 residue that is normally involved in ATP-binding by forming hydrogen bonds to the phosphate groups also interacts with coumestrol.

**Table 2**  
Kinase profiling of coumestrol (40  $\mu$ M).

Kinase	Activity	Kinase	Activity	Kinase	Activity	Kinase	Activity	Kinase	Activity
Abl(h)	50	BRK(h)	58	CDK5/p25(h)	25	CLK3(h)	24	EphA1(h)	61
ACK1(h)	38	BrSK1(h)	6	CDK5/p35(h)	37	CLK4(h)	3	EphA2(h)	44
ALK(h)	17	BrSK2(h)	8	CDK6/cyclinD3(h)	36	cKit(h)	17	EphA3(h)	52
ALK4(h)	65	BTK(h)	10	CDK7/cyclinH/MAT1(h)	86	CSK(h)	75	EphA4(h)	79
Arg(h)	67	B-Raf(h)	25	CDK9/cyclin T1(h)	27	c-RAF(h)	24	EphA5(h)	75
AMPK $\alpha$ 1(h)	26	CaMKI(h)	49	CHK1(h)	43	cSRC(h)	50	EphA7(h)	57
AMPK $\alpha$ 2(h)	10	CaMKII $\beta$ (h)	22	CHK2(h)	17	DAPK1(h)	37	EphA8(h)	57
ARK5(h)	47	CaMKII $\gamma$ (h)	20	CK1 $\gamma$ 1(h)	22	DAPK2(h)	25	EphB2(h)	53
ASK1(h)	84	CaMKI $\delta$ (h)	40	CK1 $\gamma$ 2(h)	17	DCAMKL2(h)	72	EphB1(h)	37
Aurora-A(h)	5	CaMKII $\delta$ (h)	30	CK1 $\gamma$ 3(h)	6	DDR2(h)	93	EphB3(h)	91
Aurora-B(h)	5	CaMKIV(h)	68	CK1 $\delta$ (h)	4	DMPK(h)	77	EphB4(h)	70
Aurora-C(h)	22	CDK1/cyclinB(h)	36	CK2(h)	-1	DRAK1(h)	10	ErbB4(h)	58
Axl(h)	42	CDK2/cyclinA(h)	32	CK2 $\alpha$ 2(h)	2	DYRK2(h)	-3	FAK(h)	67
Blk(h)	11	CDK2/cyclinE(h)	33	CLK1(h)	1	eEF-2K(h)	64	Fer(h)	66
Bmx(h)	41	CDK3/cyclinE(h)	33	CLK2(h)	2	EGFR(h)	73	Fes(h)	50
FGFR1(h)	10	GRK7(h)	72	IR(h), activated	46	LIMK1(h)	58	MKK6(h)	123
FGFR2(h)	34	GSK3 $\alpha$ (h)	5	IRE1(h)	86	LKB1(h)	67	MKK7 $\beta$ (h)	84
FGFR3(h)	49	GSK3 $\beta$ (h)	4	IRR(h)	14	LOK(h)	20	MLCK(h)	18
FGFR4(h)	66	Haspin(h)	2	IRAK1(h)	38	Lyn(h)	12	MLK1(h)	10
Fgr(h)	22	Hck(h)	8	IRAK4(h)	21	LRRK2(h)	91	Mnk2(h)	1
Flt1(h)	10	Hck(h) activated	11	Itk(h)	52	MAPK1(h)	72	MRCCK $\alpha$ (h)	77
Flt3(h)	5	HIPK1(h)	15	JAK1(h)	43	MAPK2(h)	45	MRCCK $\beta$ (h)	65
Flt4(h)	3	HIPK2(h)	6	JAK2(h)	49	MAPKAP-K2(h)	58	MSK1(h)	26
Fms(h)	59	HIPK3(h)	6	JAK3(h)	16	MAPKAP-K3(h)	76	MSK2(h)	8
Fyn(h)	22	IGF-1R(h)	65	JNK1 $\alpha$ 1(h)	81	MEK1(h)	76	MSSK1(h)	33
GCK(h)	4	IGF-1R(h), activated	52	JNK2 $\alpha$ 2(h)	91	MARK1(h)	67	MST1(h)	32
GCN2(h)	81	IKK $\alpha$ (h)	69	JNK3(h)	28	MELK(h)	28	MST2(h)	4
GRK1(h)	83	IKK $\beta$ (h)	54	KDR(h)	5	Mer(h)	16	MST3(h)	31
GRK5(h)	74	IKK $\epsilon$ (h)	48	Lck(h)	31	Met(h)	29	MST4(h)	46
GRK6(h)	82	IR(h)	70	Lck(h) activated	31	MINK(h)	15	mTOR(h)	82
mTOR/FKBP12(h)	65	PAR-1 $\beta$ (h)	43	PKC $\beta$ I(h)	84	PRAK(h)	26	Rsk4(h)	35
MuSK(h)	57	PASK(h)	9	PKC $\beta$ II(h)	89	PRK2(h)	37	SAPK2a(h)	99
NEK2(h)	87	PEK(h)	77	PKC $\gamma$ (h)	80	PrKX(h)	44	SAPK2b(h)	78
NEK3(h)	76	PDGFR $\alpha$ (h)	39	PKC $\delta$ (h)	79	PTK5(h)	28	SAPK3(h)	62
NEK6(h)	30	PDGFR $\beta$ (h)	53	PKC $\epsilon$ (h)	95	Pyk2(h)	38	SAPK4(h)	61
NEK7(h)	60	PDK1(h)	33	PKC $\eta$ (h)	86	Ret(h)	5	SGK(h)	19
NEK9(h)	11	PhK $\gamma$ 2(h)	19	PKC $\zeta$ (h)	91	RIPK2(h)	7	SGK2(h)	30
NEK11(h)	32	Pim-1(h)	1	PKC $\mu$ (h)	42	ROCK-I(h)	57	SGK3(h)	14
NLK(h)	18	Pim-2(h)	9	PKC $\theta$ (h)	68	ROCK-II(h)	25	SIK(h)	46
p70S6K(h)	9	Pim-3(h)	6	PKC $\zeta$ (h)	69	Ron(h)	45	Snk(h)	34
PAK1(h)	46	PKA(h)	57	PKD2(h)	25	Ros(h)	89	SRPK1(h)	60
PAK2(h)	70	PKB $\alpha$ (h)	52	PKG1 $\alpha$ (h)	13	Rse(h)	61	SRPK2(h)	82
PAK4(h)	67	PKB $\beta$ (h)	44	PKG1 $\beta$ (h)	13	Rsk1(h)	15	STK25(h)	82
PAK5(h)	34	PKB $\gamma$ (h)	18	Plk1(h)	58	Rsk2(h)	19	STK33(h)	22
PAK6(h)	48	PKC $\alpha$ (h)	80	Plk3(h)	33	Rsk3(h)	46	Syk(h)	33
TAK1(h)	46	Tie2(h)	38	Txk(h)	40	VRK2(h)	68	PI3 Kinase (p110 $\alpha$ /p85 $\alpha$ )(h)	75
TAO1(h)	23	TLK2(h)	75	TYK2(h)	25	Yes(h)	23	PI3KC2 $\alpha$ (h)	87
TAO2(h)	26	TrkA(h)	13	ULK2(h)	74	ZAP-70(h)	86	PI3KC2 $\gamma$ (h)	44
TAO3(h)	38	TrkB(h)	30	ULK3(h)	67	ZIPK(h)	21	PIP4K2 $\alpha$ (h)	89
TBK1(h)	58	TrkC(h)	17	Wee1(h)	78	PI3 Kinase (p110 $\beta$ /p85 $\alpha$ )(h)	79	PIP5K1 $\alpha$ (h)	70
Tec(h) activated	27	TSSK1(h)	27	WNK2(h)	42	PI3 Kinase (p120 $\gamma$ )(h)	79	PIP5K1 $\gamma$ (h)	88
TGFB $\beta$ 1(h)	90	TSSK2(h)	35	WNK3(h)	60	PI3 Kinase (p110 $\delta$ /p85 $\alpha$ )(h)	78		

Upon binding of coumestrol, the side chain of Phe830 of the DFG-motif is stabilized and defined in the electron density with the plane of the phenyl-ring oriented perpendicular to the plane of the coumestrol-molecule (Fig. 4D). The thermodynamic and kinetic data of coumestrol-FLT3 binding are similar to those of the commercial inhibitor 4-APIA.

Phosphorylation of MAPKs, including ERK, JNK, and p38, promotes expression or activation of AP-1 [9]. Coumestrol down-regulates ERK phosphorylation level by inhibiting c-Raf phosphorylation and suppresses Akt/p70<sup>S6K</sup> phosphorylation. PI3K and its downstream target p70<sup>S6K</sup> are closely related to the UVB-induced

MMP-1 and MMP-3 expression in fibroblasts [10]. Moreover serine/threonine protein kinase Akt, a downstream effector of PI3K, is activated by UVB [34,45] and the Akt/p70<sup>S6K</sup> signal cascade is subsequently stimulated. Finally phosphorylated Akt increases transcription of genes for MMP-1, MMP-3, and MMP-9 through up-regulated AP-1 activity [10,46,47]. Taken together, coumestrol regulates the FLT3 signaling pathway, reduces elevated levels of AP-1 activity, and inhibits MMP-1 gene transcription. In addition, we show that the modes of modulation of the FLT3 pathway by the pharmacological inhibitor 4-APIA and by coumestrol have a close resemblance.

**Table 3**  
Kinase screening of coumestrol (5  $\mu$ M).

Kinase	Activity	Kinase	Activity	Kinase	Activity	Kinase	Activity	Kinase	Activity
ALK(h)	59	CK2(h)	5	GSK3 $\alpha$ (h)	14	Mer(h)	48	Pim-2(h)	56
AMPK $\alpha$ 2(h)	78	CK2 $\alpha$ 2(h)	14	GSK3 $\beta$ (h)	30	MINK(h)	41	Pim-3(h)	36
Aurora-A(h)	68	CLK1(h)	10	Haspin(h)	3	MLCK(h)	43	PKB $\gamma$ (h)	99
Aurora-B(h)	35	CLK2(h)	24	Hck(h)	67	MLK1(h)	57	PKG1 $\alpha$ (h)	41
Blk(h)	85	CLK4(h)	6	Hck(h) activated	47	Mnk2(h)	9	PKG1 $\beta$ (h)	48
BrSK1(h)	42	cKit(h)	32	HIPK1(h)	43	MSK2(h)	78	Ret(h)	41
BrSK2(h)	50	DRAK1(h)	45	HIPK2(h)	38	MST2(h)	41	RIPK2(h)	18
BTK(h)	67	DYRK2(h)	16	HIPK3(h)	46	NEK9(h)	83	Rsk1(h)	61
CaMKII $\gamma$ (h)	61	FGFR1(h)	77	IRR(h)	30	NLK(h)	46	Rsk2(h)	80
CHK2(h)	67	Flt1(h)	32	JAK3(h)	99	p70S6K(h)	58	SGK(h)	95
CK1 $\gamma$ 2(h)	67	Flt3(h)	13	KDR(h)	20	PASK(h)	53	SGK3(h)	103
CK1 $\gamma$ 3(h)	74	Flt4(h)	8	LOK(h)	79	PhK $\gamma$ 2(h)	70	TrkA(h)	30
CK1 $\delta$ (h)	27	GCK(h)	13	Lyn(h)	71	Pim-1(h)	16	TrkC(h)	81

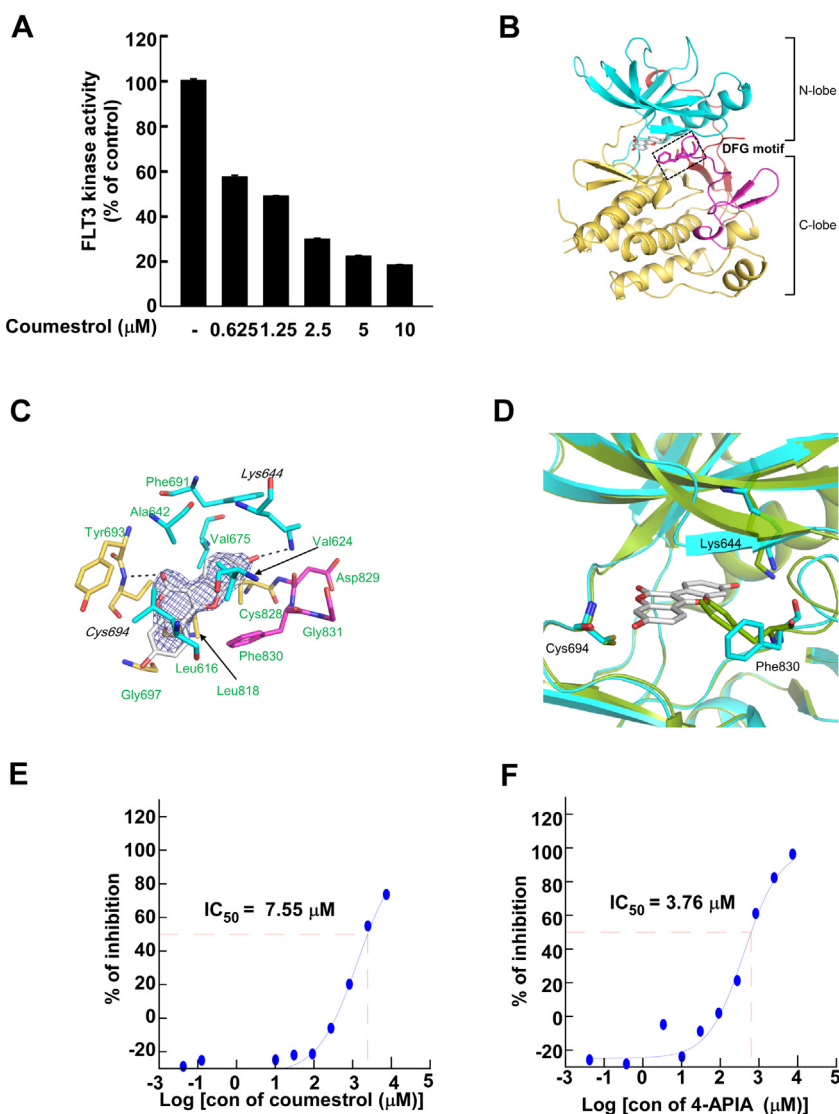


**Fig. 4.** Effect of coumestrol on FLT3 kinase activity and the FLT3-coumestrol complex structure. (A) Coumestrol decreased FLT3 kinase activity *in vitro*. Data are the means  $\pm$  S. D. ( $n = 3$ ). (B) Overall structure of the FLT3-coumestrol complex. The kinase domain of FLT3 consists of N-lobe, C-lobe, the activation loop (magenta), and juxtamembrane domain (red). The DFG motif is shown as a stick-representation. (C) The molecular interactions between coumestrol and FLT3. Hydrophobic interactions, green; hydrogen bonding, italics; hydrogen bonds, black dashed lines. (D) Enlarged view of the catalytic pocket of FLT3. Apo-FLT3, cyan; the complex with coumestrol, green. E and F, binding kinetics of the FLT3 with coumestrol (E) and 4-APIA (F) with the reporter displacement assay. Each experiment was performed in triplicate. (For interpretation of the references to color in this figure legend, the reader is referred to the web version of this article.)

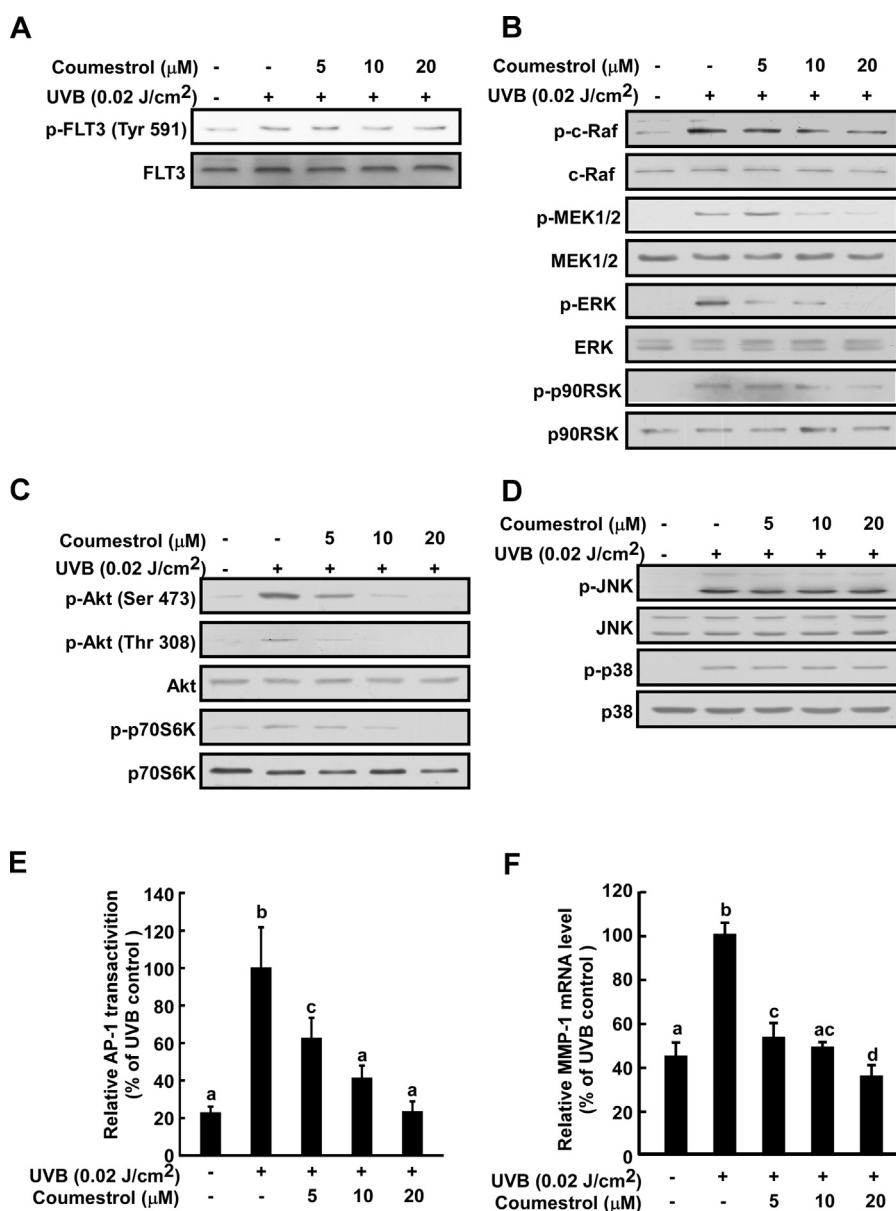


**Fig. 5.** Inhibitory effect of coumestrol on UVB-induced signaling pathways. (A)–(D) After coumestrol treatment and UVB irradiation on HDFs, phosphorylated and total form of indicated proteins was determined by Western blot. Total form of each protein was used as a loading control. All data are representative of three independent experiments that gave similar results. (E) AP-1 transactivation ability was measured using a Luciferase assay. (F) MMP-1 mRNA level of coumestrol was analyzed by Real-time RT-PCR. (E) and (F), Data are the means  $\pm$  S.D. ( $n=3$ ). Means with different letters (a–d) within a graph were significantly different from each other at  $p < 0.05$ .

3D human skin equivalent model has been developed to replace animal experiments for cosmetic materials [48] and was shown to have physiologically comparable properties to the real skin [49]. It is generated from primary human keratinocytes on a collagen substrate containing human dermal fibroblasts [50]. It is grown at the air-liquid interface where epidermal-dermal interactions to occur and allows full epidermal stratification. 3D human skin equivalent is also used to characterize the mode of action of novel agents and their efficacy in skin [49]. It is regarded as a valid alternative for animal testing with numerous applications.

In conclusion, we elucidated a novel role of coumestrol in preventing skin wrinkle formation and its effect was superior compared to its precursors daidzin and daidzein. Coumestrol regulates Ras/MEK/ERK and Akt/p70<sup>S6K</sup> pathway through targeting FLT3 kinase, which results in suppression of the MMP-1 transcription by decreasing AP-1 activity. Moreover, we established the relationship between MMP-1 expression and the FLT3 pathway for

the first time. We suggest coumestrol as a beneficial agent in preventing photoaging and the FLT3 kinase as a potential therapeutic target of wrinkle formation.

#### Disclosure

None.

#### Acknowledgements

This work was supported by the Leap Research Program of the National Research Foundation funded by the Bio-industry Technology Development Program (514004) funded by the Ministry of Agriculture, Food and Rural Affairs and the R&D program of MOTIE/KIAT (Establishment of Infra Structure for Anti-aging Industry Support, N0000697) of Republic of Korea.

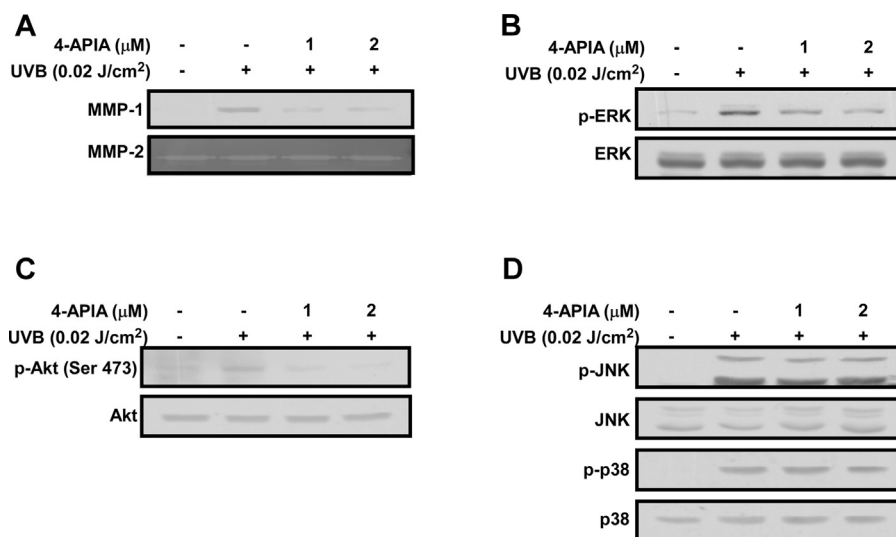


**Fig. 6.** FLT3 inhibitor 4-APIA regulates MMP-1 expression by inhibiting ERK and Akt pathway. (A) The effect of 4-APIA on UVB-induced MMP-1 expression. After 1 h of 4-APIA treatment, 0.02 J/cm<sup>2</sup> UVB was irradiated on the cells. The media were collected after 2 days and MMP-1 expression was detected by Western blot. MMP-2 expression was used as loading control. (B)–(D) The effect of 4-APIA on MAPKs and Akt phosphorylation. After 4-APIA treatment and UVB irradiation on the cells, phosphorylated and total form of indicated proteins was determined by Western blot. Total form of each protein was used as loading control. All data were representative of three independent experiments that gave similar results.

## References

- [1] G. Jenkins, Molecular mechanisms of skin ageing, *Mech. Ageing Dev.* 123 (2002) 801–810.
- [2] J.H. Chung, Photoaging in Asians, *Photodermatol. Photoimmunol. Photomed.* 19 (2003) 109–121.
- [3] Y. Matsumura, H.N. Ananthaswamy, Toxic effects of ultraviolet radiation on the skin, *Toxicol. Appl. Pharmacol.* 195 (2004) 298–308.
- [4] K. Biniek, K. Levi, R.H. Dauskardt, UV Solar radiation reduces the barrier function of human skin, *Proc. Nat. Acad. Sci. U. S. A.* 109 (2012) 17111–17116.
- [5] G.J. Fisher, S.C. Datta, H.S. Talwar, Z.Q. Wang, J. Varani, S. Kang, et al., Molecular basis of sun-induced premature skin ageing and retinoid antagonism, *Nature* 379 (1996) 335–339.
- [6] G. Fisher, Z. Wang, S. Datta, J. Varani, S. Kang, J. Voorhees, Pathophysiology of premature skin aging induced by ultraviolet light, *N. Engl. J. Med.* 1997 (1997) 20.
- [7] J. Uitto, M.J. Fazio, D.R. Olsen, Molecular mechanisms of cutaneous aging: age-associated connective tissue alterations in the dermis, *J. Am. Acad. Dermatol.* 21 (1989) 614–622.
- [8] J. Chung, J. Seo, H. Choi, M. Lee, C. Youn, G. Rhie, et al., Modulation of skin collagen metabolism in aged and photoaged human skin *in vivo*, *J. Invest. Dermatol.* 117 (2001) 1218–1224.
- [9] A.J. Whitmarsh, R.J. Davis, Transcription factor AP-1 regulation by mitogen-activated protein kinase signal transduction pathways, *J. Mol. Med. (Berlin, Germany)* 74 (1996) 589–607.
- [10] P. Brenneisen, Activation of p70 Ribosomal protein s6 kinase is an essential step in the dna damage-dependent signaling pathway responsible for the ultraviolet B-mediated increase in interstitial collagenase (MMP-1) and stromelysin-1 (MMP-3) protein levels in human dermal fibroblasts, *J. Biol. Chem.* 275 (2000) 4336–4344.
- [11] A. Murkies, G. Wilcox, S. Davis, Phytoestrogens, *J. Clin. Endocrinol. Metab.* 83 (1998) 297–303.
- [12] R. Simons, H. Gruppen, T.F. Bovee, M.A. Verbruggen, J.P. Vincken, Prenylated isoflavonoids from plants as selective estrogen receptor modulators (phytoSERMs), *Food Function* 3 (2012) 810–827.
- [13] R. Simons, J.P. Vincken, M.C. Bohin, T.F. Kuijpers, M.A. Verbruggen, H. Gruppen, Identification of prenylated pterocarpan and other isoflavonoids in *Rhizopus* spp. elicited soya bean seedlings by electrospray ionisation mass spectrometry, *Rapid Commun. Mass Spectrom.* RCM 25 (2011) 55–65.
- [14] M. Kurosu, Soybean and health: biologically active molecules from soybeans, *InTech* (2011) 2011.
- [15] H.Y. Jeon, D.B. Seo, H.J. Shin, S.J. Lee, Effect of *Aspergillus oryzae*-challenged germination on soybean isoflavone content and antioxidant activity, *J. Agric. Food Chem.* 60 (2012) 2807–2814.
- [16] J.H. Lee, B.W. Lee, J.H. Kim, T.S. Jeong, M.J. Kim, W.S. Lee, et al., LDL-antioxidant pterocarpan from roots of *Glycine max* (L.) Merr, *J. Agric. Food Chem.* 54 (2006) 2057–2063.
- [17] J.H. Lee, B.W. Lee, J.H. Kim, T.-S. Jeong, M.J. Kim, W.S. Lee, et al., LDL-antioxidant pterocarpan from roots of *Glycine max* (L.) Merr, *J. Agric. Food Chem.* 54 (2006) 2057–2063.
- [18] C. Canal Castro, A.S. Pagnussat, L. Orlandi, P. Worm, N. Moura, A.M. Etgen, et al., Coumestrol has neuroprotective effects before and after global cerebral ischemia in female rats, *Brain Res.* 1474 (2012) 82–90.
- [19] Y.H. Lee, H.J. Yuk, K.H. Park, Y.S. Bae, Coumestrol induces senescence through protein kinase CKII inhibition-mediated reactive oxygen species production in human breast cancer and colon cancer cells, *Food Chem.* 141 (2013) 381–388.
- [20] C. Taxvig, I.O. Specht, J. Boberg, A.M. Vinggaard, C. Nellemann, Dietary relevant mixtures of phytoestrogens inhibit adipocyte differentiation *in vitro*, *Food Chem. Toxicol.* 55 (2013) 265–271.
- [21] W. Kabsch, XDS, *Acta Crystallogr. D Biol. Crystallogr.* 66 (2010) 125–132.
- [22] J. Griffith, J. Black, C. Faerman, L. Swenson, M. Wynn, F. Lu, et al., The structural basis for autoinhibition of FLT3 by the juxtamembrane domain, *Mol. Cell* 13 (2004) 169–178.
- [23] A. Vagin, A. Teplyakov, Molecular replacement with MOLREP, *Acta Crystallogr. D Biol. Crystallogr.* 66 (2010) 22–25.
- [24] P. Emsley, K. Cowtan, Coot model-building tools for molecular graphics, *Acta Crystallogr. D Biol. Crystallogr.* 60 (2004) 2126–2132.
- [25] A.A. Vagin, R.A. Steiner, A.A. Lebedev, L. Potterton, S. McNicholas, F. Long, et al., REFMAC5 dictionary: organization of prior chemical knowledge and guidelines for its use, *Acta Crystallogr. D Biol. Crystallogr.* 60 (2004) 2184–2195.
- [26] L. Neumann, A. Ritscher, G. Muller, D. Hafenbradl, Fragment-based lead generation: identification of seed fragments by a highly efficient fragment screening technology, *J. Comput.-Aided Mol. Des.* 23 (2009) 501–511.
- [27] M. Uhlen, P. Oksvold, L. Fagerberg, E. Lundberg, K. Jonasson, M. Forsberg, et al., Towards a knowledge-based human protein atlas, *Nature Biotechnol.* 28 (2010) 1248–1250.
- [28] L. Neumann, K. von Konig, D. Ullmann, HTS reporter displacement assay for fragment screening and fragment evolution toward leads with optimized binding kinetics, binding selectivity, and thermodynamic signature, *Methods Enzymol.* 493 (2011) 299–320.
- [29] D.R. Knighton, J.H. Zheng, L.F. Ten Eyck, V.A. Ashford, N.H. Xuong, S.S. Taylor, et al., Crystal structure of the catalytic subunit of cyclic adenosine monophosphate-dependent protein kinase, *Science* 253 (1991) 407–414.
- [30] Y. Dai, K. Hartandi, Z. Ji, A.A. Ahmed, D.H. Albert, J.L. Bauch, et al., Discovery of *N*-(4-(3-amino-1H-indazol-4-yl)phenyl)-*N'*-(2-fluoro-5-methylphenyl) urea (ABT-869), a 3-aminoindazole-based orally active multitargeted receptor tyrosine kinase inhibitor, *J. Med. Chem.* 50 (2007) 1584–1597.
- [31] M. Dosit, S. Wang, I.R. Lemischka, Mitogenic signalling and substrate specificity of the Flk2/Flt3 receptor tyrosine kinase in fibroblasts and interleukin 3-dependent hematopoietic cells, *Mol Cell Biol.* 13 (1993) 6572–6585.
- [32] S. Takahashi, Inhibition of the MEK/MAPK signal transduction pathway strongly impairs the growth of Flt3-ITD cells, *Am. J. Hematol.* 81 (2006) 154–155.
- [33] S. Takahashi, Downstream molecular pathways of FLT3 in the pathogenesis of acute myeloid leukemia: biology and therapeutic implications, *J. Hematol. Oncol.* 4 (2011) 13.
- [34] Y. Ibuki, R. Goto, Suppression of apoptosis by UVB irradiation: survival signaling via PI3-kinase/Akt pathway, *Biochem. Biophys. Res. Commun.* 279 (2000) 872–878.

- [35] P. Brenneisen, H. Sies, K. Scharffetter-Kochanek, Ultraviolet-B irradiation and matrix metalloproteinases: from induction via signaling to initial events, *Ann. N. Y. Acad. Sci.* 973 (2002) 31–43.
- [36] G. Fisher, S. Kang, J. Varani, Z. Bata-Csorgo, Y. Wan, S. Datta, et al., Mechanisms of photoaging and chronological skin aging, *Arch Dermatol.* 138 (2002) 1462–1470.
- [37] M.D. Sternlicht, Z. Werb, How matrix metalloproteinases regulate cell behavior, *Ann. Rev. Cell Dev. Biol.* 17 (2001) 463–516.
- [38] M. Brennan, H. Bhatti, K.C. Nerusu, N. Bhagavathula, S. Kang, G.J. Fisher, et al., Matrix metalloproteinase-1 is the major collagenolytic enzyme responsible for collagen damage in UV-irradiated human skin, *Photochem. Photobiol.* 78 (2003) 43–48.
- [39] L. Chen, J.Y. Hu, S.Q. Wang, The role of antioxidants in photoprotection: a critical review, *J. Am. Acad. Dermatol.* 67 (2012) 1013–1024.
- [40] L. Rittié, G.J. Fisher, UV-light-induced signal cascades and skin aging, *Ageing Res. Rev.* 1 (2002) 705–720.
- [41] G. Di Carlo, N. Mascolo, A.A. Izzo, F. Capasso, Flavonoids old and new aspects of a class of natural therapeutic drugs, *Life Sci.* 65 (1999) 337–353.
- [42] K.W. Lee, A.M. Bode, Z. Dong, Molecular targets of phytochemicals for cancer prevention, *Nat. Rev. Cancer* 11 (2011) 211–218.
- [43] D.L. Stirewalt, J.P. Radich, The role of FLT3 in haematopoietic malignancies, *Nat. Rev. Cancer* 3 (2003) 650–665.
- [44] A. Hachiya, A. Kobayashi, A. Ohuchi, Y. Takema, G. Imokawa, The paracrine role of stem cell factor/c-kit signaling in the activation of human melanocytes in ultraviolet-B-induced pigmentation, *J. Invest. Dermatol.* 116 (2001) 578–586.
- [45] C. Kuhn, S.A. Hurwitz, M.G. Kumar, J. Cotton, D.F. Spandau, Activation of the insulin-like growth factor-1 receptor promotes the survival of human keratinocytes following ultraviolet B irradiation, *Int. J. Cancer* 80 (1999) 431–438.
- [46] J.H. Oh, A. Kim, J.M. Park, S.H. Kim, A.S. Chung, Ultraviolet B-induced matrix metalloproteinase-1 and -3 secretions are mediated via PTEN/Akt pathway in human dermal fibroblasts, *J. Cell. Physiol.* 209 (2006) 775–785.
- [47] P. Angel, A. Szabowski, M. Schorpp-Kistner, Function and regulation of AP-1 subunits in skin physiology and pathology, *Oncogene* 20 (2001) 2413–2423.
- [48] E.H. van den Bogaard, G.S. Tjabringa, I. Joosten, M. Vonk-Bergers, E. van Rijnssen, H.J. Tijssen, et al., Crosstalk between keratinocytes and T cells in a 3D microenvironment: a model to study inflammatory skin diseases, *J. Invest. Dermatol.* 134 (2014) 719–727.
- [49] H. Mertsching, M. Weimer, S. Kersen, H. Brunner, Human skin equivalent as an alternative to animal testing, *GMS Krankenhaushygiene interdisziplinär* 3 (2008) Doc11.
- [50] S. Nayak, S. Dey, S.C. Kundu, Skin equivalent tissue-engineered construct: co-cultured fibroblasts/ keratinocytes on 3D matrices of sericin hope cocoons, *PLoS one* 8 (2013) e74779.